Iron Clusters

International Edition: DOI: 10.1002/anie.201505671
German Edition: DOI: 10.1002/ange.201505671

Synthesis of Well-Defined Bicapped Octahedral Iron Clusters $[(^{tren}L)_2Fe_8(PMe_2Ph)_2]^n$ ($n = 0, -1$)

*Raúl Hernández Sánchez, Alexander M. Willis, Shao-Liang Zheng, and Theodore A. Betley**

Abstract: *The synthesis of polynuclear clusters with control over size and cluster geometry remains an unsolved challenge. Herein, we report the synthesis and characterization of open-shell octairon clusters supported by two heptaamine ligands [o-$H_2NC_6H_4NH(CH_2)_2]_3N$ ($^{tren}LH_9$). The crystal structure of the all-ferrous species ($[^{tren}L)_2Fe_8(PMe_2Ph)_2]$ (**1**) displays a bicapped octahedral geometry with Fe–Fe distances ranging from 2.4071(6) to 2.8236(5) Å, where the ligand amine units are formally in amine, amide, and imide oxidation states. Several redox states of the octairon cluster are accessible, as ascertained using cyclic voltammetry. The one-electron-reduced clusters $[M]^+[(^{tren}L)_2Fe_8(PMe_2Ph)_2]^-$ ($M = Bu_4N$ (**2a**); (15-crown-5)Na(thf) (**2b**)) were isolated and characterized. Variable-temperature magnetic susceptibility data indicates that the exchange coupling within the $[Fe_8]$ core is antiferromagnetic which is attenuated upon reduction to the mixed valent anion.*

Polynuclear metal clusters have significant utility in nature to perform transformations of high complexity (for example, small-molecule-activation catalysis).[1] Nature's polynuclear catalysts have multiple metal centers at the reaction site that facilitate substrate binding and activation[2] as well as multi-electron delivery.[3] The cluster catalysts are hosted within a protein framework that maintains the metallocofactor structural integrity.[4] In the absence of the protein superstructure, the synthetic chemist must rely on ligands to serve as the cluster template. The synthesis of polynuclear clusters in a predictable manner has been an active research area over the last four decades.[5] Cluster synthesis remains far from programmatic[6] as most successful cluster syntheses rely heavily on the principles of self-assembly and are, thus, highly dependent on metal precursor, solvent, and temperature, where small alterations can result in drastically different products.[5h,l,7] To address this challenge, we present herein our efforts to synthesize well-defined, high-nuclearity clusters.

Previous work from our lab demonstrates the feasibility of synthesizing tri-[8] and hexanuclear[9] clusters embedded within multidentate ligand scaffolds featuring multiple metal-binding sites. The parent $^{H}LH_6$ ligand [(*o*-$NH_2C_6H_4NHCH_2)_3CMe$] contains three *ortho*-phenylenediamine (OPDA) units connected using a C_3-symmetric backbone. Upon double deprotonation of each of the OPDA subunits, $^{H}L^{6-}$ can bind three divalent metal ions. We envisioned that incorporation of an additional metal binding site would potentially afford clusters of higher nuclearity. To this end tris(2-aminoethyl)amine (tren), was functionalized at the primary amine positions by a nucleophilic aromatic substitution with *o*-fluoronitrobenzene (4 equiv K_2CO_3, MeCN, 120 °C). The bright-orange product [*o*-$NO_2C_6H_4NH(CH_2)_2]_3N$ was then reduced under a H_2 pressure of 90 psi at 60 °C over 5% Pd/C in THF to form the corresponding heptaamine [*o*-$H_2NC_6H_4NH(CH_2)_2]_3N$ ($^{tren}LH_9$) in good yield (9.7 g; 79%).

Metallation of $^{tren}LH_9$ in the presence of 2 equivalents of $[Fe_2(Mes)_4]$ (Mes = mesityl) and 1 equivalent of dimethylphenylphosphine (PMe_2Ph) afforded in 59% yield the octanuclear $[(^{tren}L)_2Fe_8(PMe_2Ph)_2]$ (**1**) cluster that has a bicapped octahedral metal core geometry (Scheme 1). Crystals suitable for single-crystal X-ray diffraction were grown from

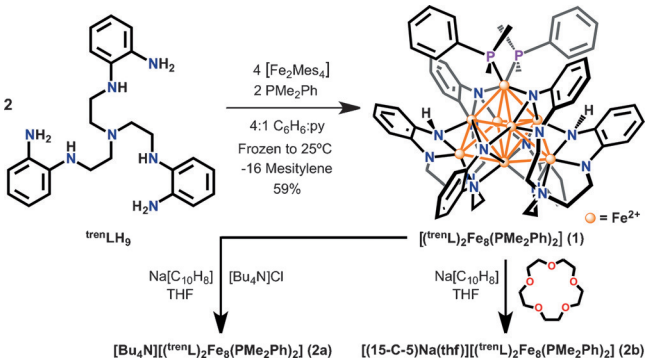

Scheme 1. Synthesis of $[(^{tren}L)_2Fe_8(PMe_2Ph)_2]$ and its anion. Py = pyridine.

a concentrated solution of **1** in THF:Et_2O at room temperature. The molecular crystal structure of $[(^{tren}L)_2Fe_8(PMe_2Ph)_2]$ (**1**) shown in Figure 1a has a C_2 axis that runs through the Fe1 atom (the phosphine-bound iron site) and the *trans*-disposed Fe6 site. Thus, crystallographically **1** contains five different iron sites: the phosphine-bound iron center, Fe1; the *trans*-disposed iron site (with respect to Fe1), Fe6; any two adjacent iron centers in the equatorial positions of the bicapped octahedron, for example, Fe2 and Fe3; and the iron center capping the central octahedron, Fe7. The molecular structure of **1** reveals four 4-coordinate iron sites: the phosphine-bound site Fe1, Fe6, and the iron sites bound to the tertiary central amine of the tren moiety Fe7 (and Fe7′). The

[*] R. H. Sánchez,[+] A. M. Willis,[+] S.-L. Zheng, Prof. T. A. Betley
Department of Chemistry and Chemical Biology
Harvard University
12 Oxford St. Cambridge, MA, 02138 USA
E-mail: betley@chemistry.harvard.edu
[+] These authors contributed equally to this work.

Supporting information for this article is available on the WWW under http://dx.doi.org/10.1002/anie.201505671.

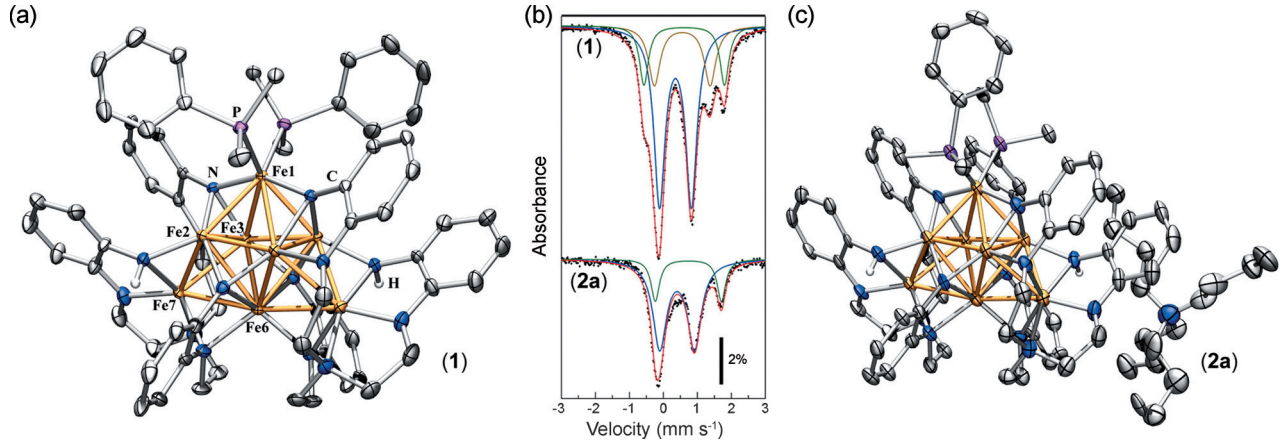

Figure 1. Molecular crystal structures of a) [(^{tren}L)$_2$Fe$_8$(PMe$_2$Ph)$_2$] (**1**) and c) [Bu$_4$N][(^{tren}L)$_2$Fe$_8$(PMe$_2$Ph)$_2$] (**2a**) with thermal ellipsoids set at 50% probability; hydrogen atoms and solvent molecules omitted for clarity. Atom colors: Fe = orange, C = gray, N = blue, H = white, P = magenta. b) Zero-field ^{57}Fe Mössbauer spectra for **1** (top) and **2a** (bottom). The black-dotted trace shows the experimentally obtained data and the red trace is an average of the model fittings. Component parameters for the model fittings of the spectrum of **1** (δ, $|\Delta E_Q|$; measured in mm s^{-1}): 0.35, *0.94* (60%, blue trace); 0.55, *1.64* (20%, brown trace); 0.61, *2.37* (20%, green trace). Parameters for the model fittings of **2a** (δ, $|\Delta E_Q|$; mm s^{-1}): 0.40, *1.02* (67%, blue trace); 0.73, *1.95* (33%, green trace).

remaining four equatorial iron sites (Fe2/Fe2′ and Fe3/Fe3′) are bound to three anilido residues making up the equatorial sites on the central octahedron. The Fe–Fe distances in **1** range from 2.4071(6) to 2.8236(5) Å.[10]

Examination of cluster **1** reveals that two ligands support an all-Fe^{II} (assigned by charge balance to the deprotonated anilide groups) octairon core. Full deprotonation of ^{tren}LH$_9$ would afford a nona-anionic ligand; nonetheless only eight ligand deprotonations occur during formation of **1**, corresponding to the stabilization of four equivalents of Fe^{II}. This ligand deprotonation state requires two primary anilido positions to be doubly deprotonated, formally creating two imido units per ligand, which has not been previously reported with these ligand types.[8b,9,11] A total of four ligand imido functionalities cap a tri-iron face in a μ^3-fashion on the Fe$_8$ cluster. For the remaining two primary anilido groups, their hydrogens were located in the electron density map (Figure 1a). In contrast to the previously reported hexanuclear clusters where two ligands forming the polynuclear species were *trans*-disposed, **1** is formed by two C_2-symmetry-related ^{tren}L^{8-} ligands sitting at the base of the iron-based bicapped octahedron. The apical iron site is bound only to two anilido groups, thus requiring the additional phosphine coligand to complete its coordination sphere.

Chemical reduction of **1** was accomplished with one equivalent of sodium naphthalenide in THF followed either by salt metathesis with [Bu$_4$N]Cl or Na$^+$ encapsulation with 15-crown-5. Salt metathesis afforded a black powder from which we were able to grow crystals of [Bu$_4$N][(^{tren}L)$_2$Fe$_8$(PMe$_2$Ph)$_2$] (**2a**), whereas Na$^+$ encapsulation afforded [(15-crown-5)Na(thf)][(^{tren}L)$_2$Fe$_8$(PMe$_2$Ph)$_2$] (**2b**). Crystals of **2a** and **2b** were grown on standing from a solution of the compound in MeCN:Et$_2$O and THF:Et$_2$O, respectively, at −35 °C. The molecular crystal structures of **2a** and **2b** are isostructural to that of **1**, apart from the countercation present to balance the charge of the one-electron reduced cluster, as shown in Figure 1c and Figure S5 in the Supporting Information, respectively.[12] The local symmetry of the [Fe$_8$]$^-$ cluster in **2a** has lost the crystallographic C_2 axis presumably because of a crystal-packing effect as the symmetry decrease appears to be due to a slight rotation of the phosphine coligands. There is no marked correlation for the Fe–Fe distances upon reduction which vary from 2.386(2) to 2.864(1) Å in **2a** (Figure S6).

Both neutral **1** and its reduced congener **2a** were investigated by zero-field ^{57}Fe Mössbauer spectroscopy. Polycrystalline samples were immobilized in Paratone-N oil and their spectra were recorded at 90 K. The spectrum of **1** displays three distinct Fe environments (Figure 1b, top), although five distinct geometry environments are expected from the single-crystal molecular structure. By modeling the spectrum as such the component metrical parameters δ (isomer shift; mm s^{-1}) and $|\Delta E_Q|$ (quadrupole splitting (in italics); mm s^{-1}) can be determined. For compound **1** the following parameters were determined (δ, $|\Delta E_Q|$; mm s^{-1}): 0.35, *0.94* (60%, blue trace); 0.55, *1.64* (20%, brown trace); and 0.61, *2.37* (20%, green trace). Based on the composition of **1** and the similarities of the local coordination environments of the iron centers therein, we propose that iron atoms Fe2–Fe7 give rise to the lower isomer shift doublets ($\delta = 0.35$, 0.55 mm s^{-1}), whereas the higher isomer shift site ($\delta =$ 0.61 mm s^{-1}) is likely attributable to the phosphine-bound Fe1 center. These metrical parameters are consistent with those obtained for previously reported Fe^{II} clusters,[8,9] specifically the high-spin Fe^{II} clusters bearing a similar N-rich ligand environment supported by tertiary phosphine ancillary ligation,[13] but are also in range with parameters obtained for amide-based Fe^{III} clusters.[14] The Mössbauer spectrum of **2a** is almost identical to that of **1** with only one major difference: the intermediate isomer-shift iron environment has merged with the main component (blue trace). Thus, as shown in Figure 1b (bottom), the fitting of the spectrum of **2a** displays two components (δ, $|\Delta E_Q|$ (mm s^{-1}): 0.40, *1.02* (67%) and 0.73, *1.95* (33%)). The increase in isomer shifts to higher

velocities is consistent with the overall reduction of the iron valency states, suggesting delocalization of the added electron (see below).

The redox reversibility of **1** was investigated by electrochemical methods. Towards this end cyclic voltammetry on a THF solution of **1** revealed an open-circuit potential of −1.30 V and a reversible reduction at $E_{1/2} = -1.52$ V (all potentials reported versus Ag/Ag^+; see Figure S12). Given the improved solubility of **2b** in THF, we surmised that better electrochemical kinetics could be obtained with the monoanionic cluster $[Fe_8]^-$. Cyclic voltammetric analysis of **2b** displayed an open-circuit potential of −1.80 V confirming thus the assignment of a one-electron event at $E_{1/2} = -1.52$ V as a reduction event. As expected the cyclic voltammogram of **2b** displays the same redox events as **1** with the exception that the couple $[Fe_8]^-/[Fe_8]^{2-}$ ($E_{1/2} = -2.11$ V) becomes rigorously reversible (Figure 2a), followed by a poorly defined second reduction at circa −2.8 V. In the anodic scan three oxidations are detected. The first one is reversible at −1.49 V ($[Fe_8]/[Fe_8]^-$) followed by two irreversible oxidations at $E_{pa} = -0.75$ and −0.52 V. The irreversible electrochemical oxidation behavior provides a potential reason why attempted chemical oxidations of **1** were unsuccessful. The redox events between −1.10 and −2.50 V were confirmed to be fully reversible by scanning at various rates (10 and 150 mV s^{-1}) and fitting the resulting peak current density (j_p) to the Randles–Sevcik equation (Figure 2b).[15] The diffusion coefficient (D_s) of a molecule in solution is well known to give an indirect measure of its size.[16] From the above data the extracted D_s is $4.5(5) \times 10^{-6}$ $cm^2 s^{-1}$, which lies between the size typical of small molecules such as ferrocene (2×10^{-5} $cm^2 s^{-1}$)[17] and large macromolecules such as dendrimers (1×10^{-7} $cm^2 s^{-1}$).[18]

The determination of the electronic structure of metal cofactors in biological systems has provided insight into the nature of intermediates and their potential mechanism of action.[19] In synthetic cluster systems a wider range of spectroscopic and magnetic techniques are available for electronic structure determination that are otherwise inaccessible to biological cofactors. We thus explored the magnetic properties of **1** and **2a** by acquiring variable-temperature magnetic susceptibility data collected on heating from 5 to 300 K in 5 K increments (1 T dc field, Figure 2c). The purity of the complexes was ascertained by checking the linearity of the magnetization data at 100 K (to rule out ferromagnetic impurities, see Figures S13, S14) and from the superimposable $\chi_M T$ data (χ_M = magnetic susceptibility) at two different applied dc fields (Figure S15). At 300 K the all-Fe^{II} species **1** and the one-electron-reduced compound **2a** have $\chi_M T$ values of 12.7 and 18.4 $cm^3 K mol^{-1}$, respectively. These values are significantly smaller than those expected for eight non-interacting Fe^{II} high-spin $S = 2$ centers (24 $cm^3 K mol^{-1}$, $g = 2.0$) in the case of **1**, or seven $S = 2$ and one $S = {}^3/_2$ iron centers (22.875 $cm^3 K mol^{-1}$, $g = 2.0$) in the case of **2a**. The magnetic behavior across the temperature range investigated displays a monotonic decrease of $\chi_M T$ values for both **1** and **2a** as the temperature is lowered. At 5 K **1** and **2a** have $\chi_M T$ values of 2.68 and 3.55 $cm^3 K mol^{-1}$, respectively. This behavior indicates antiferromagnetic coupling within the $[Fe_8]$ cluster core. Unfortunately, the VT magnetic susceptibility data could not be modeled employing the Kambe method[20] as pointed out by Belorizky and Fries[21] for an octahedral bicapped geometry. Instead the reciprocal molar magnetic susceptibility ($1/\chi_M$) was fitted to the Curie–Weiss law, $1/\chi_M = (T-\theta)/C$ (Figure 2c). Data in the range 150–300 K was fit in this manner. The Curie constants obtained were $C =$ 21.3 and 22.1 $cm^3 K mol^{-1}$ with Weiss constants θ of −204.3 and −61.7 for **1** and **2a**, respectively. Although the actual magnitude of the magnetic interactions within the octanuclear cluster could not be obtained, the Weiss constants clearly point towards strong antiferromagnetic interactions in **1**. It is interesting to note that the value of θ in **2a** is significantly smaller; in addition to the overall geometry and metal–metal distances not changing from that of the neutral species **1**, this indicates that the itinerant electron within the octanuclear core attenuates the antiferromagnetic exchange

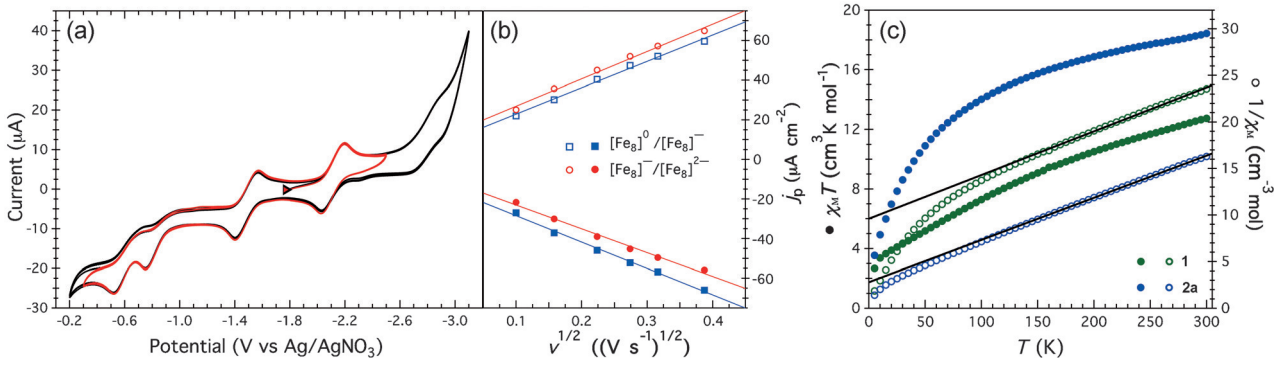

Figure 2. a) Cyclic voltammetry of $[(15\text{-crown-5})Na(thf)][(^{tren}L)_2Fe_8(PMe_2Ph)_2]$ (**2b**; red and black traces). The black trace is included to show that the poorly defined reduction at −2.8 V does not affect the remaining redox processes (red trace). Both voltammograms were collected at 20 mV s^{-1} and with 0.1 M $[Bu_4N]PF_6$ as the supporting electrolyte in THF. b) Cathodic (open symbols) and anodic (filled symbols) current density versus the square root of the scan rate for $E_{1/2}$ values at −1.49 (blue) and −2.11 V (red) versus $Ag/AgNO_3$. c) Variable-temperature dc magnetic susceptibility of $[(^{tren}L)_2Fe_8(PMe_2Ph)_2]$ (**1**; green symbols); and $[Bu_4N][(^{tren}L)_2Fe_8(PMe_2Ph)_2]$ (**2a**; blue symbols). Both datasets were collected at 0.5 T. $\chi_M T$ values (solid symbols) and the reciprocal molar magnetic susceptibility ($1/\chi_M$, open symbols) versus temperature are shown on the left and right vertical axis, respectively.

interaction because of electron delocalization by double exchange.[22]

Efforts to elucidate the ground state of these clusters were carried out by collecting variable-temperature (VT), variable-field (VH) magnetization studies as well as VT electron paramagnetic resonance spectra. The reduced magnetization data of **1** could be fit well to an $S = 2$ with fit parameters: $g = 2.16 \pm 0.01$, $|D| = 6.3 \pm 0.1\ cm^{-1}$, and $|E/D| = 0.30 \pm 0.03$ (Figure S16), where D and E are the axial and rhombic zero-field splitting constants, respectively. In the case of **2a** magnetization saturation occurs at 4.79 μ_B at 1.8 K and 7 T, close to the expected value of 5.0 μ_B for an ideal $S = {}^5/_2$ ($g = 2.0$) in the absence of zero-field splitting. Despite several fitting strategies, we were not able to find a satisfactory model to reproduce the VTVH magnetization data of **2a** (Figure S17). Similarly, the X-band VT EPR spectra are complex with multiple transitions between 200 and 1700 Gauss for which we currently do not have an interpretation (Figure S18).

From our previous research on the synthesis of polynuclear complexes we have learned that well-defined octahedral hexanuclear clusters can be prepared by dimerization of two trinuclear units supported by hexamine ligands.[9,11] In the present report we expanded the ligand backbone into a tetraamine moiety by use of tren to accommodate a fourth metal per ligand, affording bicapped octahedral octanuclear clusters. Prediction of polynuclear cluster geometry can be made by use of Wade's rules,[23] later expanded by Lewis et al.[24] to polycarbonyl clusters. Predictions by Wade's rules are applicable to many cluster types and nuclearities.[25] The reported species **1** and **2a**,**b** do not strictly follow these rules as the calculated number of skeletal electron pairs (Sk) is 6 or 8 (although 7 is the expected number).[26] This discrepancy may be in part as a result of the geometry restriction imposed by the $^{tren}L^{8-}$ ligand in contrast to the self-assembled polycarbonyl clusters, which relax to the respective thermodynamically stable configuration. In fact, there are no reported[27] bicapped octahedral molecular clusters for first-row transition-metal (TM) homonuclear clusters, though examples with second-row TM[7b,28] and third-row TM,[24b,29] as well as one heterobimetallic $[Os_6Pt_2]$ cluster,[30] are known. Thus, the ligand framework reported herein allowed us to synthesize octairon clusters with a rare cluster configuration and redox tunability.

In conclusion, octairon clusters **1** and **2a**,**b** display open-shell configurations with metal–metal interactions that feature antiferromagnetic coupling. The coupling is significantly attenuated in the mixed-valence species **2a**, potentially as a result of delocalization of the itinerant electron. The synthetic strategy adopted herein to increase cluster nuclearity may be employed to synthesize even larger assemblies with some control on geometry and size.

Acknowledgements

This research was supported by the NIH (GM 098395), Harvard University, and a George W. Merck Fellowship for T.A.B. R.H.S. acknowledges Consejo Nacional de Ciencia y Tecnología (CONACYT) and Fundación México for a doctoral fellowship.

Keywords: cluster compounds · cyclic voltammetry · iron · magnetic properties · structure elucidation

How to cite: *Angew. Chem. Int. Ed.* **2015**, *54*, 12009–12013
Angew. Chem. **2015**, *127*, 12177–12181

[1] a) O. Einsle, F. A. Tezcan, S. L. A. Andrade, B. Schmid, M. Yoshida, J. B. Howard, D. C. Rees, *Science* **2002**, *297*, 1696–1700; b) K. N. Ferreira, T. M. Iverson, K. Maghlaoui, J. Barber, S. Iwata, *Science* **2004**, *303*, 1831–1838; c) Y. L. Hu, M. W. Ribbe, *J. Biol. Inorg. Chem.* **2014**, *19*, 731–736; d) T. Happe, A. Hemschemeier, *Trends Biotechnol.* **2014**, *32*, 170–176.

[2] a) A. Messerschmidt, R. Ladenstein, R. Huber, M. Bolognesi, L. Avigliano, R. Petruzzelli, A. Rossi, A. Finazziagro, *J. Mol. Biol.* **1992**, *224*, 179–205; b) J. H. Jeoung, H. Dobbek, *Science* **2007**, *318*, 1461–1464.

[3] L. C. Seefeldt, B. M. Hoffman, D. R. Dean, *Curr. Opin. Chem. Biol.* **2012**, *16*, 19–25.

[4] G. Berggren, A. Adamska, C. Lambertz, T. R. Simmons, J. Esselborn, M. Atta, S. Gambarelli, J. M. Mouesca, E. Reijerse, W. Lubitz, T. Happe, V. Artero, M. Fontecave, *Nature* **2013**, *499*, 66–69.

[5] a) H. Vahrenkamp, V. A. Uchtman, L. F. Dahl, *J. Am. Chem. Soc.* **1968**, *90*, 3272–3273; b) P. D. Frisch, L. F. Dahl, *J. Am. Chem. Soc.* **1972**, *94*, 5082–5084; c) Trinh-Toan, W. P. Fehlhammer, L. F. Dahl, *J. Am. Chem. Soc.* **1972**, *94*, 3389–3397; d) M. A. Neuman, Trinh-Toan, L. F. Dahl, *J. Am. Chem. Soc.* **1972**, *94*, 3383–3388; e) T. Madach, H. Vahrenkamp, *Chem. Ber./Recl.* **1981**, *114*, 505–512; f) C. T. W. Chu, F. Y. K. Lo, L. F. Dahl, *J. Am. Chem. Soc.* **1982**, *104*, 3409–3422; g) T. Saito, N. Yamamoto, T. Yamagata, H. Imoto, *J. Am. Chem. Soc.* **1988**, *110*, 1646–1647; h) D. Fenske, A. Grissinger, M. Loos, J. Magull, *Z. Anorg. Allg. Chem.* **1991**, *598*, 121–128; i) G. Aromí, J. P. Claude, M. J. Knapp, J. C. Huffman, D. N. Hendrickson, G. Christou, *J. Am. Chem. Soc.* **1998**, *120*, 2977–2978; j) N. T. Tran, M. Kawano, L. F. Dahl, *J. Chem. Soc. Dalton Trans.* **2001**, 2731–2748; k) N. R. M. Crawford, J. R. Long, *Inorg. Chem.* **2001**, *40*, 3456–3462; l) T. G. Gray, *Coord. Chem. Rev.* **2003**, *243*, 213–235; m) I. Chakraborty, P. Baran, Y. Sanakis, A. Simopoulos, E. Fachini, R. G. Raptis, *Inorg. Chem.* **2008**, *47*, 11734–11737.

[6] J. R. Long, A. S. Williamson, R. H. Holm, *Angew. Chem. Int. Ed. Engl.* **1995**, *34*, 226–229; *Angew. Chem.* **1995**, *107*, 248–251.

[7] a) B. A. Averill, T. Herskovitz, R. H. Holm, J. A. Ibers, *J. Am. Chem. Soc.* **1973**, *95*, 3523–3534; b) M. Bochmann, I. Hawkins, M. B. Hursthouse, R. L. Short, *Polyhedron* **1987**, *6*, 1987–1991; c) E. J. Laskowski, R. B. Frankel, W. O. Gillum, G. C. Papaefthymiou, J. Renaud, J. A. Ibers, R. H. Holm, *J. Am. Chem. Soc.* **1978**, *100*, 5322–5337; d) T. E. North, J. B. Thoden, B. Spencer, A. Bjarnason, L. F. Dahl, *Organometallics* **1992**, *11*, 4326–4337; e) T. E. North, J. B. Thoden, B. Spencer, L. F. Dahl, *Organometallics* **1993**, *12*, 1299–1313; f) S. C. Lee, R. H. Holm, *Chem. Rev.* **2004**, *104*, 1135–1157; g) P. V. Rao, R. H. Holm, *Chem. Rev.* **2004**, *104*, 527–559; h) J. L. Krinsky, L. L. Anderson, J. Arnold, R. G. Bergman, *Inorg. Chem.* **2008**, *47*, 1053–1066.

[8] a) T. M. Powers, A. R. Fout, S. L. Zheng, T. A. Betley, *J. Am. Chem. Soc.* **2011**, *133*, 3336–3338; b) Q. L. Zhao, T. A. Betley, *Angew. Chem. Int. Ed.* **2011**, *50*, 709–712; *Angew. Chem.* **2011**, *123*, 735–738.

[9] a) Q. L. Zhao, T. D. Harris, T. A. Betley, *J. Am. Chem. Soc.* **2011**, *133*, 8293–8306; b) T. D. Harris, Q. L. Zhao, R. Hernández Sánchez, T. A. Betley, *Chem. Commun.* **2011**, *47*, 6344–6346.

[10] Crystallographic information for compound **1** can be found in Table S1 and in CCDC 1405825. These data can be obtained free

of charge from The Cambridge Crystallographic Data Centre via www.ccdc.cam.ac.uk/data_request/cif.
[11] A. R. Fout, Q. L. Zhao, D. N. J. Xiao, T. A. Betley, *J. Am. Chem. Soc.* **2011**, *133*, 16750 – 16753.
[12] Crystallographic information for compounds **2a** and **2b** can be found in Table S1 and in CCDC 1405824 and 1405823. These data can be obtained free of charge from The Cambridge Crystallographic Data Centre via www.ccdc.cam.ac.uk/data_request/cif.
[13] E. V. Eames, T. D. Harris, T. A. Betley, *Chem. Sci.* **2012**, *3*, 407 – 415.
[14] a) H. Link, A. Decker, D. Fenske, *Z. Anorg. Allg. Chem.* **2000**, *626*, 1567 – 1574; b) A. K. Verma, T. N. Nazif, C. Achim, S. C. Lee, *J. Am. Chem. Soc.* **2000**, *122*, 11013 – 11014; c) J. S. Duncan, T. M. Nazif, A. K. Verma, S. C. Lee, *Inorg. Chem.* **2003**, *42*, 1211 – 1224; d) J. S. Duncan, M. J. Zdilla, S. C. Lee, *Inorg. Chem.* **2007**, *46*, 1071 – 1080.
[15] A. J. Bard, L. R. Faulkner, *Electrochemical Methods*: *Fundamentals and Applications*, *2nd ed.*, Wiley Global Education, New Delhi, **2000**.
[16] W. J. Feng, B. Miller, G. Bakale, *J. Phys. Chem. B* **1999**, *103*, 2943 – 2947.
[17] a) C. R. Wilke, P. Chang, *AIChE J.* **1955**, *1*, 264 – 270; b) N. G. Tsierkezos, *J. Solution Chem.* **2007**, *36*, 289 – 302.
[18] J. I. Goldsmith, K. Takada, H. D. Abruna, *J. Phys. Chem. B* **2002**, *106*, 8504 – 8513.
[19] B. M. Barney, D. Lukoyanov, R. Y. Igarashi, M. Laryukhin, T. C. Yang, D. R. Dean, B. M. Hoffman, L. C. Seefeldt, *Biochemistry* **2009**, *48*, 9094 – 9102.
[20] K. Kambe, *J. Phys. Soc. Jpn.* **1950**, *5*, 48 – 51.
[21] E. Belorizky, P. H. Fries, *J. Chim. Phys. Phys.-Chim. Biol.* **1993**, *90*, 1077 – 1100.
[22] G. Blondin, J. J. Girerd, *Chem. Rev.* **1990**, *90*, 1359 – 1376.
[23] a) K. Wade, *J. Chem. Soc. Chem. Commun.* **1971**, 792 – 793; b) K. Wade, *Inorg. Nucl. Chem. Lett.* **1972**, *8*, 559 – 562.
[24] a) C. R. Eady, B. F. G. Johnson, J. Lewis, *J. Chem. Soc. Dalton Trans.* **1975**, 2606 – 2611; b) P. F. Jackson, B. F. G. Johnson, J. Lewis, P. R. Raithby, *J. Chem. Soc. Chem. Commun.* **1980**, 60 – 61.
[25] D. M. P. Mingos, *Acc. Chem. Res.* **1984**, *17*, 311 – 319.
[26] From Ref. [24a]: The calculated number of valence electrons (VE) is 108. If the lone pair at the basal secondary amido group is considered to participate in bonding then VE = 112. It follows then that Sk = 6 (VE = 108) or Sk = 8 (VE = 112). Similarly the numbers of metal–metal bonds required for the cluster to obey the 18-electron rule are 18 and 16, respectively.
[27] I. R. Thomas, I. J. Bruno, J. C. Cole, C. F. Macrae, E. Pidcock, P. A. Wood, *J. Appl. Crystallogr.* **2010**, *43*, 362 – 366.
[28] B. F. G. Johnson, C. M. Martin, D. Braga, F. Grepioni, E. Parisini, *J. Chem. Soc. Chem. Commun.* **1994**, 1253 – 1254.
[29] A. Amoroso, B. G. Johnson, J. Lewis, C.-K. Li, C. Morewood, P. Raithby, M. Vargas, W.-T. Wong, *J. Cluster Sci.* **1995**, *6*, 163 – 173.
[30] C. Couture, D. H. Farrar, R. J. Goudsmit, *Inorg. Chim. Acta-Articles Lett.* **1984**, *89*, L29 – L30.

Received: June 19, 2015
Revised: July 2, 2015
Published online: August 19, 2015

